remote sensing

MDPI

Technical Note

Water Vapor Density Retrieval Studies Using Commercial Millimeter-Wave Links at 38 GHz and E-Band

Congzheng Han [1,2,*], Guiyang Su [3], Lei Bao [4] and Hagit Messer [5]

[1] Key Laboratory for Middle Atmosphere and Global Environment Observation (LAGEO), Institute of Atmospheric Physics, Chinese Academy of Sciences, Beijing 100029, China
[2] University of Chinese Academy of Sciences, Beijing 100049, China
[3] Zhejiang Provincial Meteorological Observatory, Hangzhou 310002, China; sgy52401314@126.com
[4] Ericsson AB, Lindholmspiren 11, 412 56 Göteborg, Sweden; lei.bao@ericsson.com
[5] School of Electrical Engineering, Tel Aviv University, Tel Aviv 6997801, Israel; messer@eng.tau.ac.il
* Correspondence: c.han@mail.iap.ac.cn

Abstract: We study the performance of water vapor monitoring using commercial millimeter-wave backhaul links from the fifth-generation cellular networks and smart cities. A 38 GHz link and an E-band link located in Gothenburg, Sweden, are used for analysis. One end of these two backhaul links is installed at the same site. The water vapor density (WVD) over a one-month period from 13 June 2017 to 13 July 2017 is calculated based on the data from these microwave links with different frequencies. The meteorological data used for analysis is from a weather station installed at the site where the microwave links are installed, as well as from a nearby weather station operated by Swedish Institute of Meteorology and Hydrology (SMHI). A pre-processing step is applied to the raw link attenuation measurement for improving the estimation accuracy. We retrieved water vapor density value from two millimeter-wave links, and it is in good agreement with the water vapor density calculated by weather stations. The source of interference, such as misalignment, humidity source below the link, location, and altitude of weather stations, can contribute to estimation errors and needs to be carefully considered when using microwave link to retrieve water vapor density.

Keywords: microwave links; millimeter-wave link; 5G; water vapor monitoring technique; E-band

Citation: Han, C.; Su, G.; Bao, L.; Messer, H. Water Vapor Density Retrieval Studies Using Commercial Millimeter-Wave Links at 38 GHz and E-Band. *Remote Sens.* **2022**, *14*, 946. https://doi.org/10.3390/rs14040946

Academic Editor: Silas Michaelides

Received: 11 December 2021
Accepted: 4 February 2022
Published: 15 February 2022

1. Introduction

Water vapor is extremely important to the weather and climate [1]. It is the most abundant greenhouse gas in the atmosphere and is also a vital component of the hydrologic cycle, and all of the water vapor that evaporates from the surface of the earth eventually returns as precipitation [2,3]. In addition, weather forecasting heavily relies on accuracy of the input measurements of atmospheric models, and accurate monitoring of water vapor has a crucial role [4,5]. However, accurate, high resolution, and global-scale measurements of water vapor are difficult to obtain.

Commonly used measurement techniques of water vapor include surface weather stations, radiosondes (balloon-borne sensors providing pressure, temperature, humidity, and wind profile data), and from satellite remote-sensed data [6–10]. Weather stations provide accurate point observations and, therefore, have low spatial representation, especially in heterogeneous terrain, or in general areas with complex topography, where limited surface stations are available. Ground-based microwave radiometers have the same issues and need to be re-calibrated during operation. Satellite remote-sensed measurement techniques, such as spaceborne infrared, GPS (global positioning system) receivers, and microwave radiometers, can provide large coverage, but its accuracy for ground monitoring is often not very high. Radiosondes offer limited coverage as they can only launch several times a day and provide observations at a small number of sites. These measurement methods have a high cost for implementation, deployment, and maintenance. Ground-based monitoring

of water vapor still poses a significant challenge, and additional data sources are very important and greatly needed.

The presence of water vapor attenuates electromagnetic radiation in the atmosphere, which is of great significance for astronomy, radar, telecommunications, and remote sensing. In recent years, innovative rainfall monitoring techniques based on terrestrial line-of-sight microwave backhaul links in commercial cellular networks have been studied and implemented in many countries [11–13]. A backhaul in the cellular network is used for providing inter-connectivity between a base station tower and the core network. As microwave and millimeter-wave links are prone to significant fading due to rain, the retrieval method is based on the empirical mathematical model for relating the rainfall rate and signal attenuation in a given link. As a result, the path-averaged rainfall rate along the microwave backhaul link can be derived from the rain-induced attenuation of the received signal measurements, and, with multiple microwave links deployed in an area, it is possible to generate a two-dimensional rain map at high tempo-spatial accuracy. This technique has already been deployed by a number of weather-services worldwide and is used as either a stand-alone tool or in combination with rain-gauges and weather radars to enhance the coverage, accuracy and resolution of the existing weather monitoring network. The ability of microwave links is not limited to rainfall monitoring, and it has been demonstrated that the potential of using microwave links to measure water vapor, as well. Electromagnetic signal attenuation due to absorption by water vapor is always present, and, particularly, the strong absorption bands of water vapor are at 22.3, 183.3, and 323.8 GHz in the microwave and millimeter-wave range [14]. Similar to rainfall rate retrieval, water vapor density can also be derived from the received signal attenuation measurements of commercial microwave backhaul links [15–17].

As the fifth generation (5G) cellular networks and smart cities technologies are being deployed over the world, they bring in new opportunities for methodological observations. While fiber-based backhaul is expensive, high speed wireless backhaul operating in the millimeter-wave range (30 to 300 GHz) is more cost-effective, flexible, and easier to deploy. The report from Ericsson has indicated that, globally, 40 percent of backhaul connections are expected to be based on microwave technology by 2023 [18].

With huge bandwidth available, wireless backhaul in millimeter-wave bands provides gigabit data rates and is promising in backhaul solutions for cities with large populations. Especially, the E-band (71–76 GHz and 81–86 GHz) is becoming an essential backhaul band of high global alignment for 5G, and it is expected to be densely deployed in cities in the future and can be usually used up to 3 km [19]. This indicates that there is potential for using new millimeter-wave backhaul links, including the E-band, to improve water vapor monitoring and provide measurement data with high resolution [20,21].

Based on commercial backhaul links at 38 GHz and the E-band, which are popular 5G frequencies, this paper studies the performance and reliability of using these links for water vapor density retrieval, compares their results, and discusses the uncertainties. We have demonstrated that short millimeter-wave links can be utilized to provide an extra rich data source for existing water vapor monitoring networks, in addition to existing monitoring methods. These measurement data can serve applications, such as weather forecasting and climate monitoring.

This paper is organized as follows. Section 2 introduces the characteristics of millimeter-wave propagation, the method of water vapor monitoring from the received signal level of links, and the setup of outdoor test links. Section 4 presents the experimental results of water vapor density retrieval studies using the low and high millimeter-wave backhaul links. Then, the uncertainties of the experiment and the potentials for the proposed technology in supporting humidity monitoring in urban areas are discussed. Finally, we summarize the work in Section 4.

2. Materials and Methods

2.1. Method for Water Vapor Density Retrieval

For a terrestrial communication link, link budget analysis is usually considered for describing how much power from the transmitter is received by the receiver and accounts for all gains and losses in the communication link [22]. For a point-to-point line-of-sight (LOS) millimeter-wave link, the received power P_R (dB) may be related to the transmitted power P_T (dBm), the propagation path loss (PL), atmospheric attenuation (AT), other losses (OL), as below:

$$P_R = P_T - PL - AT - OL(\text{dB}). \tag{1}$$

Other losses (OL) refers to the additional attenuation caused by the instrument itself, for example, the cable loss, temperature, and water vapor affecting the stability of the equipment and circuits, or anything that obstructs the LOS channel and may introduce additional loss.

The path loss of transmitted signal as a function of distance with a 1-m reference distance can be expressed as [22]:

$$PL(f,d)(\text{dB}) = FSPL(f,1\text{m})(\text{dB}) + 10nlog_{10}(d) + \chi_\sigma\ ,\ d\ \geq 1\text{m}, \tag{2}$$

where f denotes the carrier frequency in GHz, d is the transmitter and receiver separation distance, the reference distance is 1 m, and n is the path loss exponent. X_σ is a zero mean Gaussian random variable with a standard deviation in dB for modeling the large-scale shadow fading caused by large obstacles [22,23]. $FSPL$ (f, 1 m) represents the free space path loss in dB at a transmitter and receiver distance of 1 m at the carrier frequency:

$$FSPL(f,1\text{ m})(\text{dB}) = 20log_{10}\left(\frac{4\pi f \times 10^9}{c}\right) + GT + GR\ , \tag{3}$$

where c is the speed of light (3×10^8 m/s). G_T is the transmit antenna gain (dBi), and G_R is the receive antenna gain (dBi). The transmit and receive antennas are assumed to have equal gain, i.e., $G_T = G_R$. The path loss exponent n is a parameter describing how the path loss increases as the transmitter-receiver separation distance increases above the reference separation distance. In free space, n equals to 2, but, typically, n is greater than 2 because free space is an optimistic environment. In outdoor LOS measurements at millimeter-wave frequencies, n has found to be between 1.8 to 2.2.

The atmospheric and weather-related attenuation is represented by AT (dB). At millimeter-wave, the molecular constituency of air and water plays an important role in characterizing the free space propagation. AT can be modeled as:

$$\text{AT}(\text{dB}) = AT_r(\text{dB}) + AT_v(\text{dB}) + AT_o(\text{dB}) + AT_p(\text{dB}) + AT_{wa}(\text{dB}), \tag{4}$$

where AT_r is the path-integrated rain attenuation, AT_v is the attenuation due to atmospheric water vapor, AT_o is attenuation due to dry air (for millimeter-wave bands, the main absorbing gas is oxygen), AT_p refers to other weather-related attenuation, such as fog, snow, and sleet, and AT_{wa} refers to the wetness on antenna surface.

The attenuation per kilometer distance due to dry air A_0 (dB/km) and water vapor A_w (dB/km) is modeled in ITU-R P.676, as follows [24]:

$$Y = A_w + A_0\ (\text{dB/km}) = \frac{4\pi f N''}{c}\left(\text{m}^{-1}\right) = 0.1820 f N''(p,T,\rho,f)(\text{dB/km}), \tag{5}$$

where f denotes the millimeter-wave link frequency in GHz, and N'' is the imaginary part of the complex refractivity which is a function of pressure p (hPa), link frequency f (GH), temperature T (°C), and the water vapor density ρ (g/m^3).

Excess attenuation due to oxygen absorption occurs at the frequency range of 57–64 GHz. At other frequencies, up to 100 GHz, the signal attenuation due to oxygen absorption is

negligible. To illustrate the electromagnetic signal attenuation due to water vapor, Figure 1 is plotted based on the equations given in References [24–26] for typical links of 1 km length as a function of link frequency at a given barometric pressure and temperature. The absorption band of water vapor is near 22 GHz. The attenuation is estimated based on an ITU model assuming the temperature is 15 °C, and the atmospheric pressure is 1013 hPa in the environment.

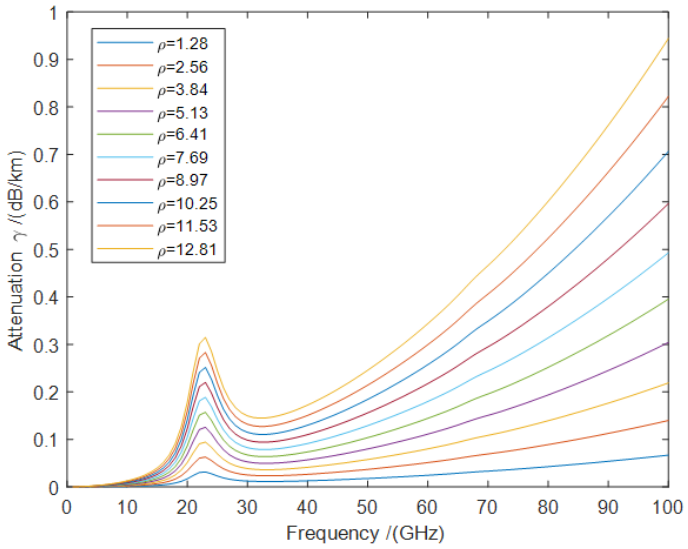

Figure 1. Transmission loss due to water vapor at the link of 1-k length. Different color curves represent different water vapor density levels, which correspond to typical humidity levels.

For fixed LOS microwave links, most of the published works [15,16] have assumed that the transmit power, transmit and receive antenna gains, free space path loss, and other losses, in Equations (1) and (2), are constants in the range of normal surface temperatures and pressure changes. In reality, temperature could affect equipment and circuits, misalignment, or anything that obstructs the LOS channel, such as birds or insects, and may introduce additional attenuation. It was a sunny day on June 27. Figure 2 shows the instantaneous transmit and receive changes of the E-band link used in this work. It shows that the received signal experiences an unexpected deep fade of 3.5 dB, while the transmit power varies due to temperature changes and adaptive transmission power control (ATPC) feature to cope with the sudden fluctuation in the received signal level in order to maintain the link quality. This sudden change in the signal level is unlikely to be caused by a change of water vapor density.

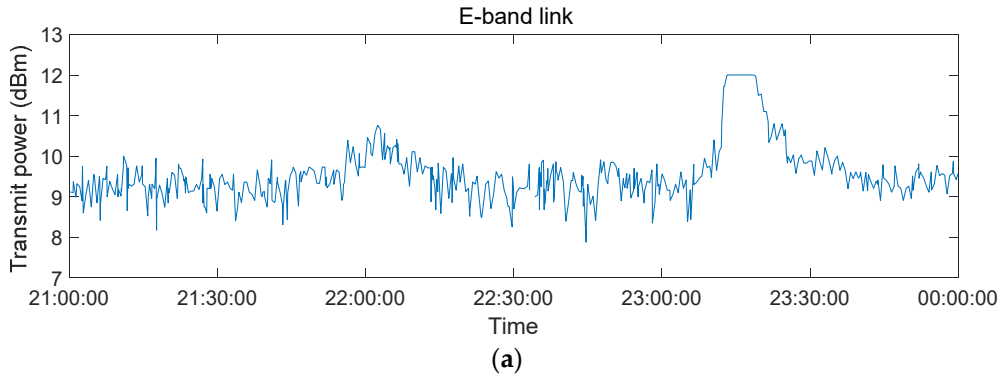

(**a**)

Figure 2. *Cont.*

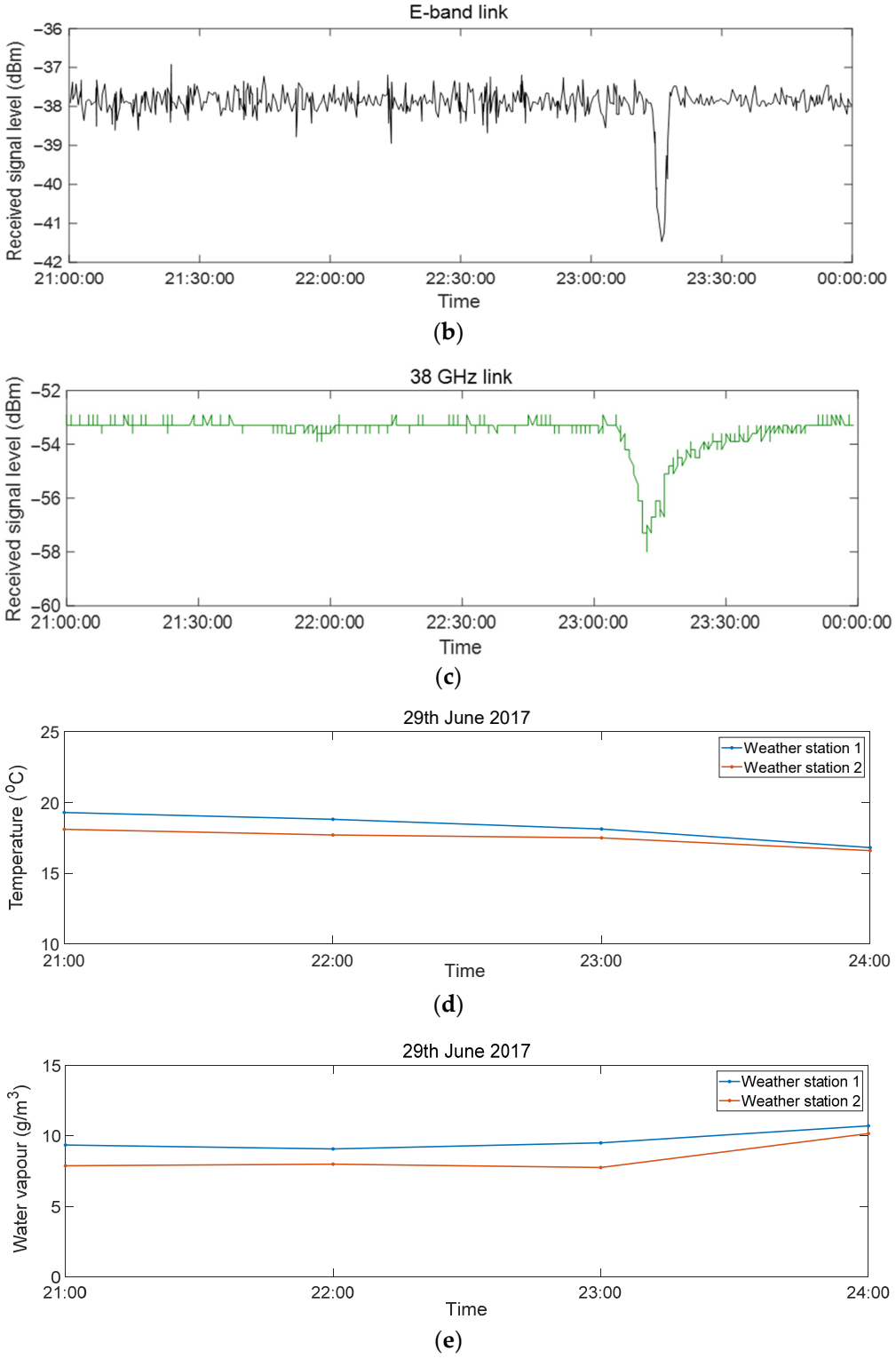

Figure 2. (**a**) Instantaneous transmit power from the transmitter of the E-band link. (**b**) Instantaneous received signal level at the receiver of the E-band link. (**c**) Instantaneous signal level received by the 38 GHz link receiver. (**d**) Temperature data recorded by nearby weather stations. (**e**) Water vapor density level measured by nearby weather stations. The experiment was carried out on 29 June 2017.

A reference received signal level (RSL) needs to be determined in advance for water vapor density retrieval study, and the corresponding WVD level is referred to as ρ_{ref}. For the kth day during the whole measurement period, assuming any atmospheric attenuation

is due to change in atmospheric humidity in a dry period, given there are a set of I measurements, the attenuation caused by the change in humidity level is given as:

$$\Delta AT_{k\_i} = AT_{k\_i} - AT_{k\_ref}, \quad (6)$$

where AT_{k_i} is ith link attenuation measurement of day k, AT_{k_ref} is the reference level on day k, and ΔAT_{k_i} is attenuation induced by the change in atmospheric humidity during the ith measurement of day k. Similar to the approach presented in Reference [27], the water vapor density is retrieved based on the actual temperature measured by the local weather station instead of the mean temperature over the whole evaluation period for improved accuracy. A pre-processing step is applied to the raw link attenuation measurement to filter out the unlikely values of attenuation. As the humidity level ranges between 0 to 100%, using Figure 1 and Table 1 as references, the maximum additional attenuation per km induced by change in humidity level with respect to the reference level $\Delta AT_{k\_i,\max}$ can be estimated. Therefore, if the measured ΔAT_{k_i} per km is greater than this maximum additional attenuation value $\Delta AT_{k\_i,\max}$, this recorded attenuation is excluded from the water vapor density retrieval study, as this attenuation is likely be caused by other issues. Figure 2b,c show examples of unexpected deep fading experienced by the 38 GHz link and the E-band link, and these data samples will be excluded from water vapor density retrieval studies as the deep fades are not caused by change of water vapor density level. After this pre-processing stage, ΔAT_{k_i} can be converted into the change of water vapor density with respect to the reference level using Equation (5), and the link-retrieved water vapor density value can be estimated based on the change of WVD and WSD reference level.

Table 1. Theoretical attenuation values (dB/km) of ITU model for typical 5G backhaul link frequencies under different humidity (%) and water vapor density levels (g/m^3).

Frequency \ Water Vapor Density/ Humidity	1.28	2.56	3.84	5.13	6.41	7.69	8.97	10.25	11.53	11.53
	10%	20%	30%	40%	50%	60%	70%	80%	90%	100%
28 GHz	0.014	0.030	0.045	0.061	0.078	0.095	0.113	0.131	0.150	0.169
38 GHz	0.013	0.026	0.040	0.055	0.072	0.089	0.107	0.125	0.145	0.166
73 GHz	0.037	0.078	0.122	0.169	0.219	0.273	0.329	0.390	0.453	0.519
83 GHz	0.048	0.100	0.156	0.217	0.281	0.350	0.424	0.501	0.582	0.668

In dry periods, the variation in attenuation due to AT_r, AT_p, and AT_{wa} are negligible. Under such conditions, the atmospheric loss is mainly due to oxygen and water vapor, i.e., the fluctuations of the received signal power P_R in Equation (1) are mainly caused by the change of AT_v in Equation (4). As a result, by monitoring the received signal power and extracting the attenuation caused by water vapor, the water vapor density can be retrieved based on Equation (5).

Since meteorological stations normally record the relative humidity, these measurements need to be converted into the water vapor density values, and their relation can be expressed as [15,24]:

$$\rho = 1324.45 \times \frac{RH}{100\%} \times exp\left(\frac{17.67T}{T+243.5}\right)/(T+273.15), \quad (7)$$

where ρ is the water vapour density (g/m^3), RH is the relative humidity recorded by weather stations (%), and T is the temperature (°C).

2.2. Statistical Performance Test

During the measurement period from 13 June 2017 to 13 July 2017, there are 21 days that have been considered for water vapor density monitoring studies, and other days with rain are excluded from our analysis. Rain can cause large attenuation over the signal link,

and wetness on the antenna due to rain induces further attenuation. In a rainy period, the relative humidity is generally quite high (often higher than 70%). According to Table 1, a change in humidity level from 70% to 100% refers to an additional attenuation of only 0.06 dB/km for the 38 GHz link, and 0.2 dB/km for the 73 GHz link. The small change in humidity during rain has little impact on the signal level, and it is very challenging to separate the attenuation caused by rainfall intensity change, water vapor density change, and other factors.

We investigate and compare the performance of water vapor density monitoring from different links using statistical tests including the Pearson correlation coefficient, root-mean-square difference, and mean and standard deviation.

The Pearson correlation coefficient (CORR) is calculated as:

$$\mathrm{CORR} = \frac{1}{N-1}\sum_{n=1}^{N}\left(\frac{X-_i-\mu_X}{\sigma_X}\right)\left(\frac{Y_i-\mu_Y}{\sigma_Y}\right), \tag{8}$$

where μ_X and σ_X are the mean and standard deviation of the link-derived water vapor density X, respectively, and μ_Y and σ_Y are the mean and standard deviation of water vapor density derived from the humidity measurement from weather station Y. $|r| \leq 1$, r ranges from -1 to +1. A correlation coefficient of +1 indicates a perfect positive correlation. A high correlation coefficient value shows better similarity between two data sets, indicating the mmW link-derived value can represent the true water vapor density well.

The root mean square difference (RMSD) is calculated as:

$$RMSD\left(\mathrm{g/m^3}\right) = \sqrt{\sum_{n=1}^{N}\frac{\left(\rho_{mi}-\rho_{gi}\right)^2}{N}}, \tag{9}$$

where ρ_{mi} is the link-derived water vapour density from the ith link measurement, ρ_{gi} is water vapor density calculated from ith humidity measurement recorded by the weather station, and N is the total number of measurements.

The bias can be calculated using the following formula:

$$Bias\left(\mathrm{g/m^3}\right) = \frac{1}{N}\sum_{n=1}^{N}\left(\rho_{mi}-\rho_{gi}\right), \tag{10}$$

and it is a measure of the average error between the link estimated water vapor density and the weather station measurement.

2.3. Outdoor Measurement

We present here a summary of the measurements of two outdoor millimeter-wave links and local weather station measurements. These measurements are also used to validate the performance of water vapor density estimation.

The measurement setup parameters are given in Table 2. One end of the 38 GHz link and the E-band link share the same site. The 38 GHz link had a length of approximately 7 km. The E-band (71–76 GHz and 81–86 GHz) was over approximately 3 km, and one end of the link is on a bridge, as shown in Figure 3. The deployment of the two microwave backhaul links is illustrated in Figure 3. Both the 38 GHz and E-band links were operated in a line-of-sight environment, and their polarization setups were vertical. All the millimeter-wave links have a sampling interval of 30 s. The microwave links have ATPC, i.e., transmitted power is automatically adjusted to minimize any fluctuations in the received signal, and, as a result, the attenuation fluctuation is smoothed.

Table 2. Outdoor measurement parameters.

Parameter	38 GHz	E-band (73 GHz)
Sampling interval	30 s	30 s
Antenna type	Cassegrain antenna	Cassegrain antenna
Location	57°42′18.97″N, 11°56′29.67″E; 57°44′52.8″N, 12°1′26.4″E	57°42′18.97″N, 11°56′29.67″E; 57°41′20.04″N, 11°54′10.76″E
Link length	6.87 km	2.9 km
Setup	SISO	SISO
Antenna no.	1 × 1	1 × 1
Antenna diameter	0.3 m	0.6 m
Antenna separation	N/A	N/A
Transmitted power	15 dBm	7 dBm
Tx antenna gain	40.3 dBi	50.5 dBi
Tx half power beam width	0.5°	0.5°
Tx polarization	V	V
Rx antenna gain	40.3 dBi	50.5 dBi
Rx half power beam width	0.5°	0.5°
Rx polarization	V	V

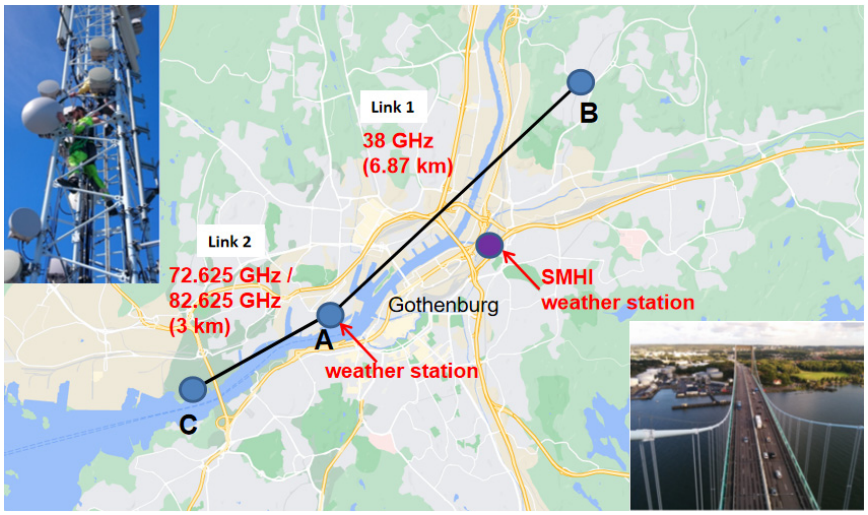

Figure 3. The deployment of two microwave backhaul links.

Temperature, humidity, air pressure, wind, and precipitation information were provided by a weather station equipped with a rain gauge located at the rooftop of shared measurement site of the two links, and it is referred to as 'weather station 1'. The accuracy of the weather station is given in Table 3 [28]. Another weather station operated by the Swedish Meteorological and Hydrological Institute (SMHI) was also considered for our analysis, referred to as 'weather station 2'. The measurement of this weather station is available on the SMHI website, and the measurement resolution is one h [29]. According to the water vapor density retrieval model, the change of pressure or temperature will not cause a significant change in the water vapor density calculation. The main uncertain factor affecting the calculation of water vapor density is the attenuation quantization error. The quantization error of the link is 0.1 dB. For the E-band link with a length of 3 km, the uncertainty of attenuation calculation is 0.03 dB/km. For the 38 GHz link with a length of 7 km, the uncertainty of attenuation calculation is 0.014 dB/km. As a result, the quantization uncertainty induced water vapor density calculation error of the E-band and 38 GHz link is approximately 0.8 g/m^3 and 1.0 g/m^3, respectively.

Table 3. The resolution, operating range, and accuracy of different weather sensors [28].

Sensor Type	Resolution	Range	Accuracy
Humidity	1%	1–100%	2%
Air pressure	0.1 mb/hPa	540 to 1100 mb/hPa	1.0 mb/hPa
Temperature	0.1 °C	−40 °C to +65 °C	0.3 °C

3. Results

The measurement period is from 13 June 2017 to 13 July 2017, data from two weather stations located in the research area were collected, and the daily statistics, including the maximum, minimum, and mean value of the temperature and water vapor density, are presented in Figure 4 for the study period. The humidity observed in the weather stations is presented in relative humidity units (%), so, in order to compare it to the link humidity, the data were converted to water vapor density, also known as absolute humidity (g/m^3). The variation in average temperature is within 0–4 °C, observed from the same weather station over this one-month period. Figure 5 presents the hourly temperature and water vapor density measured by the local weather stations. As shown in Figure 5a, the temperature data recorded by the two weather stations used for our study is similar with a correlation coefficient of 0.9. The statistics of the water vapor density obtained based on the measurement of two weather stations also have a high correlation of 0.88, as shown in Figure 4b.

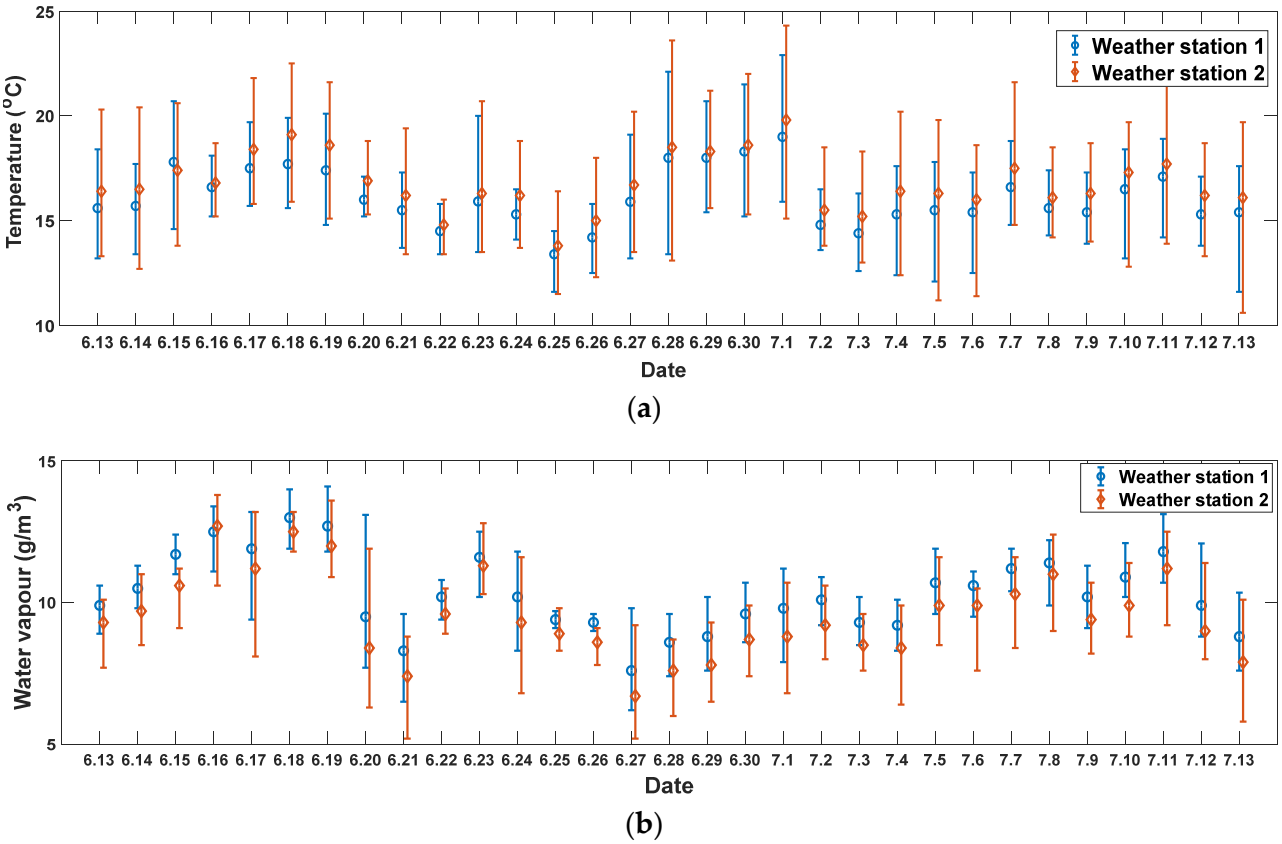

Figure 4. The maximum, minimum, and mean values of (**a**) temperature and (**b**) water vapor density measured by the weather stations every day.

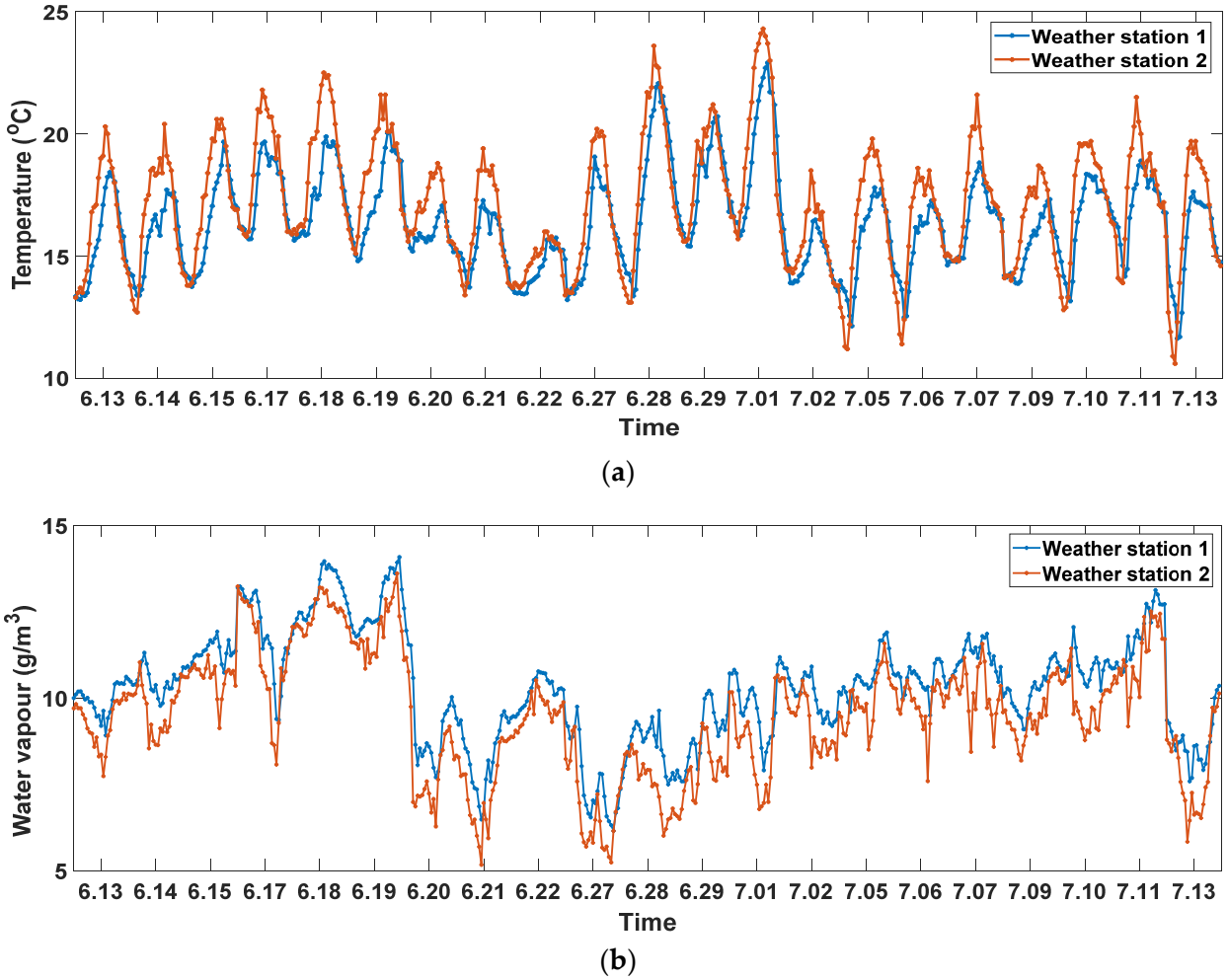

Figure 5. Correlation tests: (**a**) temperature data recorded by weather station 1 and 2; (**b**) water vapor density derived from humidity data recorded by weather station 1 and 2.

By comparing the recorded data from two different weather stations, it can be seen that there are small differences in temperature and water vapor density values at different locations in the measurement area. In order to reduce the error caused by the difference in measured locations, the meteorological data measured by weather station 1 and weather station 2 is used for evaluating the performance of water vapor density monitored by microwave link.

The water vapor density of the one-month period from 13 June 2017 to 13 July 2017 is estimated from microwave backhaul links using the method in Section 2.1. Water vapor density is retrieved every hour based on the received signal level measurement of the 38 GHz link, as presented in Figure 6. Very high correlations are found between the link retrieved WVD values and the WVD calculated based on the weather station 1 and 2 with averages of 0.83 and 0.74 as shown in Table 4. Good results are also obtained for RMSD and bias statistical scores, indicating the high quality data of using millimeter-wave link for water vapor monitoring. The link retrieved WVD shows a slightly better match with the WVD values derived from measurements recorded by weather station 1.

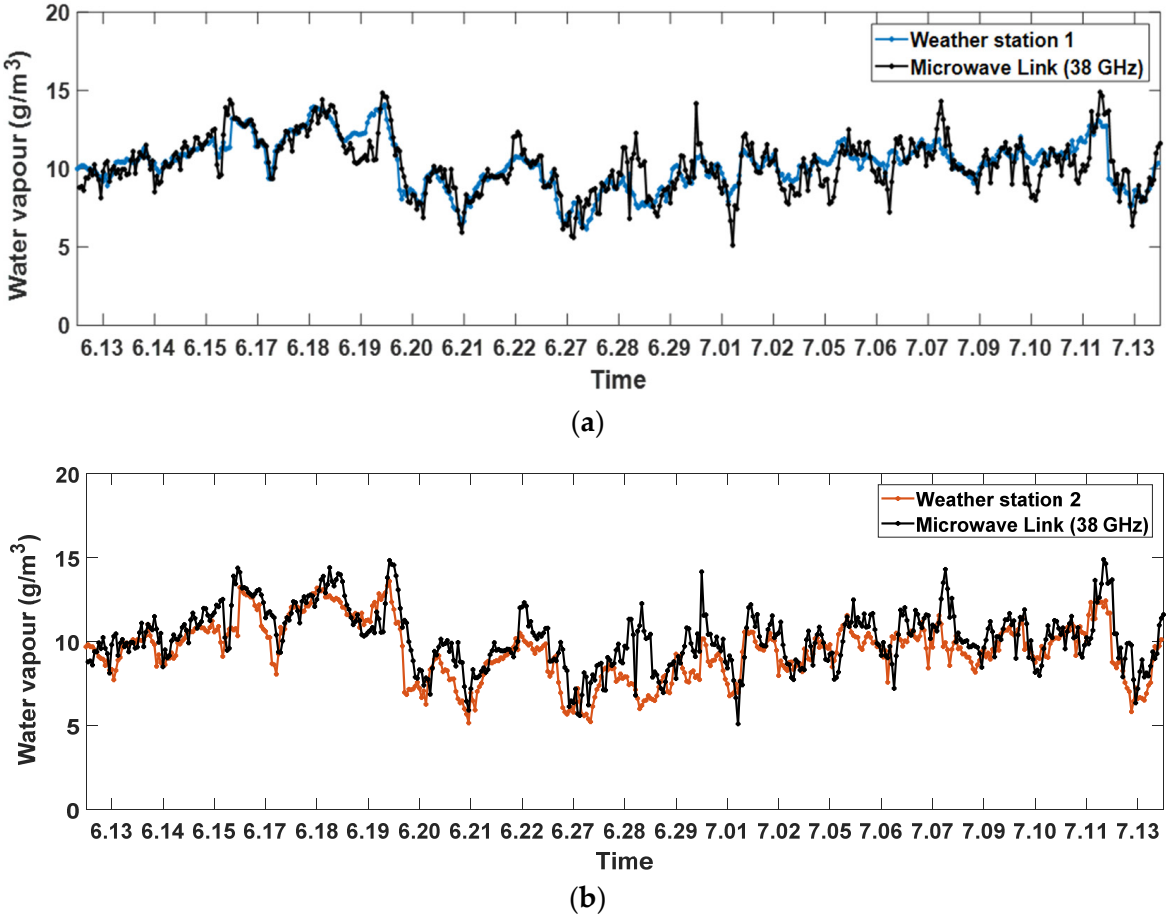

Figure 6. Water vapor density plots: (**a**) The blue line represents the change in the WVD calculated based on measurements by weather station 1 every hour, and the black line represents the derived WVD from the 38 GHz link. (**b**) The blue line represents the WVD calculated based on measurements by weather station 2, and the black line represents the derived WVD from the 38 GHz link.

Table 4. Statistical analysis of water vapor density derived from microwave links and weather station measurements.

Data Source 1	Data Source 2	Correlation	RMSD	BIAS
Weather station 1	Weather station 2	0.88	1.15	0.82
Weather station 1	38 GHz Link (24 h)	0.83	0.99	−0.04
	38 GHz Link (5 a.m.)	0.97	0.49	0.02
	E-Band Link (24 h)	0.61	1.71	0.04
	E-Band Link (5 a.m.)	0.91	0.72	0.18
Weather Station 2	38 GHz Link (24 h)	0.74	1.48	0.78
	38 GHz Link (5 a.m.)	0.77	1.18	0.59
	E-Band Link (24 h)	0.54	2.08	0.86
	E-Band Link (5 a.m.)	0.67	1.48	0.74

By comparing the estimated WVD values derived from the 38 GHz and E-band link, the results show that both links can be used for monitoring the local WVD, as illustrated in Figures 6 and 7. As one end of the 38 GHz link and E-band link are built at the rooftop of the same building, where weather station 1 is also installed, the WVD inversion results from both links are highly correlated with the WVD derived from weather station 1 measurements. Unlike weather station 1, weather station 2 is the only weather station operated by SMHI in this area, and it is not located along the experimental links, especially

further away from E-band link. As a result, the correlation between the link-derived WVD and WVD calculated from weather station 2 measurements is lower, especially for the E-band link.

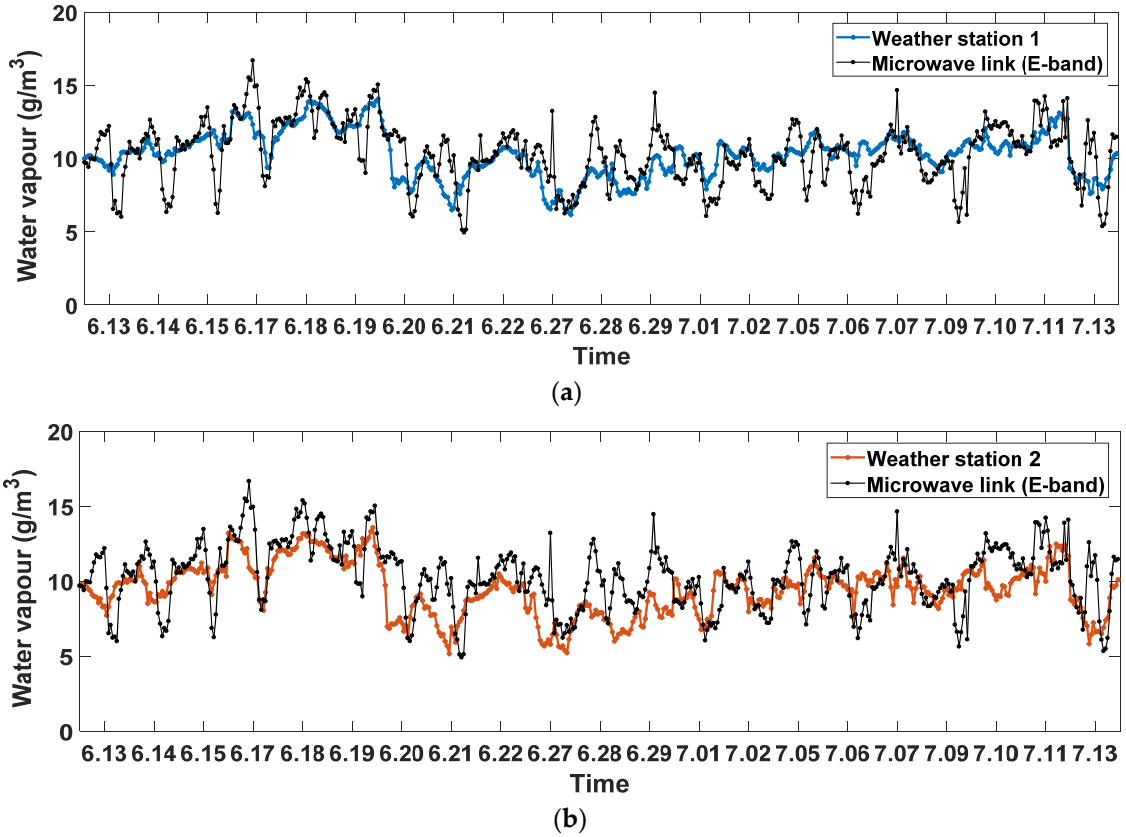

Figure 7. Water vapor density plots: (**a**) The blue line represents the change in the WVD based on measurements by weather station 1 every hour, and the black line represents the derived WVD from the E-band link. (**b**) The blue line represents the WVD calculated based on measurements by weather station 2, and the black line represents the derived WVD from the E-band link.

The overall performance of water vapor monitoring achieved by the 38 GHz link is better than the E-band link. There are several possible causes of this difference. The measurements of the microwave link are influenced by the variation in water vapor along the link, while the weather station only measures the weather conditions over a very limited area. The E-band link is built across the Gota River in Gothenburg, and this source of humidity below the link could affect the signal attenuation. There are also hardware issues; for example, temperature changes cause power variation. The antenna diameter of the E-band radio equipment is 0.6 m, which is bigger than the antenna of the 38 GHz link, and one end of the E-band link is on a bridge. As a result, it is very difficult to perform alignment, and there is often alignment mismatch due to this location. The E-band radio has adaptive transmission power control feature, which automatically increases or decreases the transmit power based on the received signal level and signal quality to maintain the reliability of the link. It is shown in Figure 2a,b that the received signal level and transmit power of the E-band link is continuously varying. Further attenuation could be caused by misalignment, and this increases the uncertainty of retrieving WVD from link. In comparison, the 38 GHz link has a fixed transmit power, and its received signal is less affected by hardware issues, as shown in Figure 2c.

In order to check the WSD retrieval quality of the two links, we choose 5:00 a.m. every day during the whole measurement period because the surrounding environment, such as traffic on the bridge and river, has less impact on the links than the peak traffic time. The

results in Figure 8 and statistics in Table 4 show that WVD values retrieved from the 38 GHz and E-band link are both in good agreement with WSD obtained from the weather station. The correlation between the E-band link retrieved WSD and WSD calculated from weather station 1 increases from 0.61 to 0.91, and the RMSD is reduced from 1.71 to 0.72 g/m^3. We also calculate statistics of WVD derived from the E-band link and the weather station for every hour of the day throughout the measurement period and present that in Table 5. It illustrates that the link-estimated water vapor density level shows better performance from midnight to early morning (7:00 a.m.) and from 11:00 a.m. till early afternoon (4:00 p.m.). These are the relatively quiet times of the day.

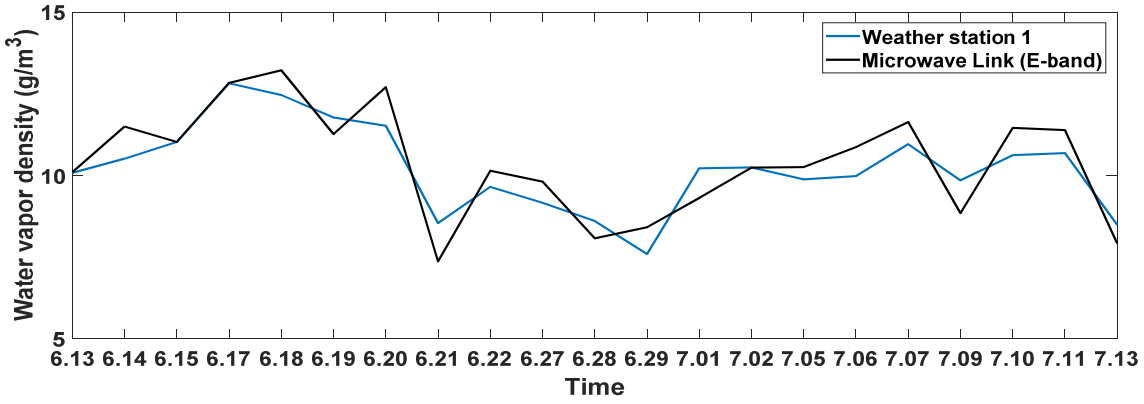

(**a**)

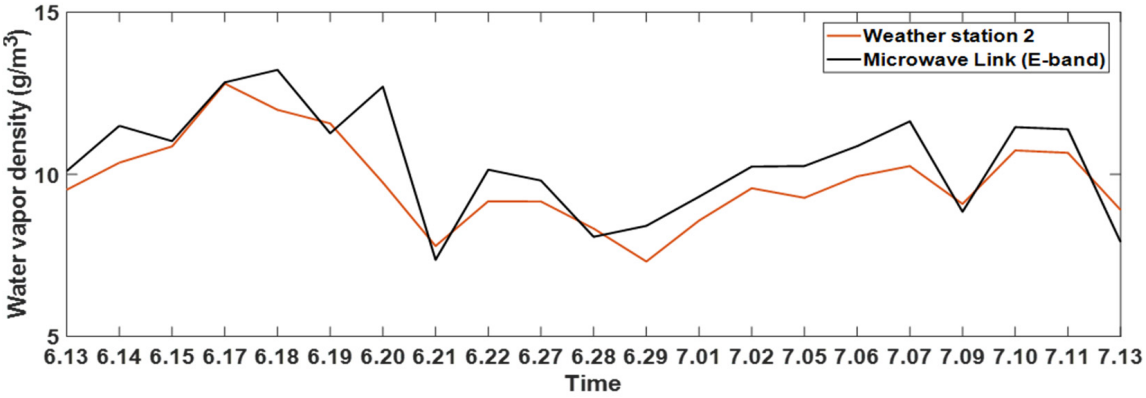

(**b**)

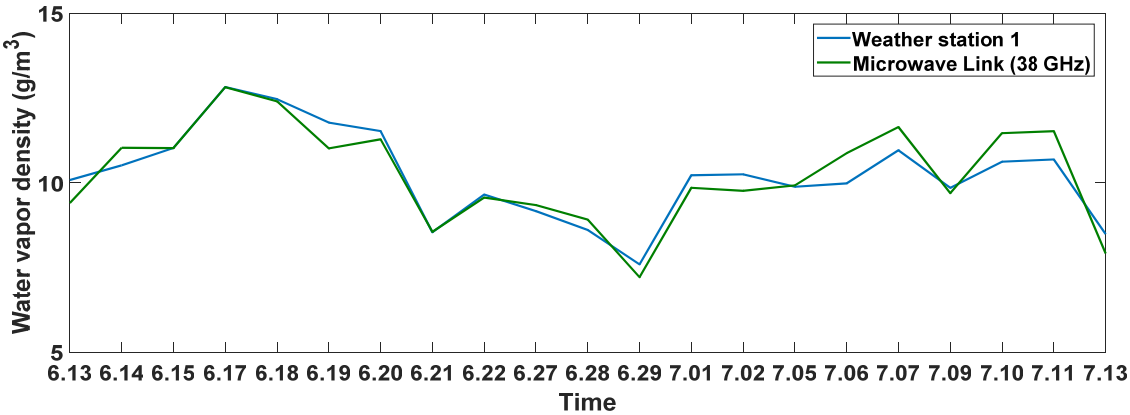

(**c**)

Figure 8. *Cont.*

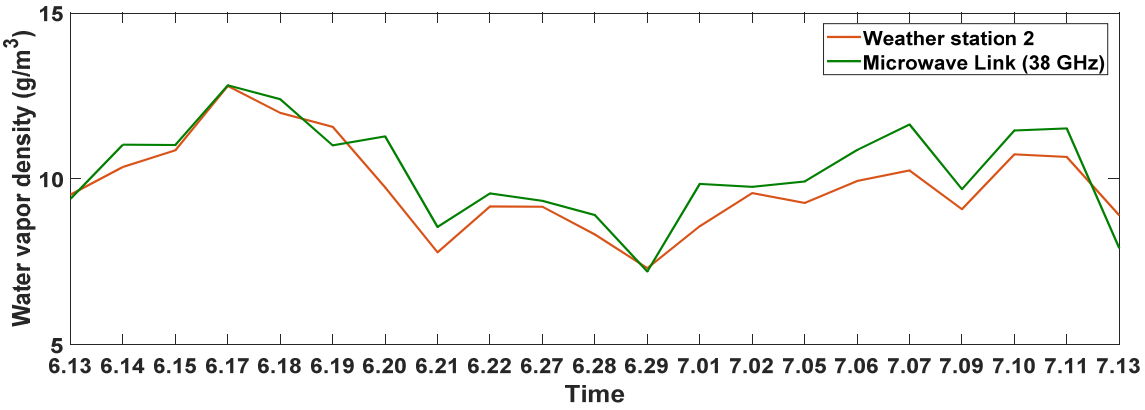

(**d**)

Figure 8. Water vapor density plots: (**a**) The WVD calculated from humidity and temperature measurements by weather station 1 at 5:00 a.m. every day during the measurement period, compared with the value derived from the E-band link. (**b**) The WVD calculated based on measurements by weather station 2 at 5:00 a.m. every day, compared with the value derived from the E-band link. (**c**) The WVD calculated based on measurements by weather station 1 at 5:00 a.m. every day, compared with the value derived from the 38 GHz link. (**d**) The WVD calculated based on measurements by weather station 2 at 5:00 a.m. every day, compared with the value derived from the 38 GHz link.

Table 5. Statistics of WVD derived from E-band link and weather station at different times during the day.

Data Source	Weather Station 1 and E-Band Link			Weather Station 2 and E-Band Link		
Time	Correlation	RMSD	BIAS	Correlation	RMSD	BIAS
1:00	0.85	0.86	−0.18	0.80	1.04	0.31
2:00	0.77	1.01	−0.18	0.72	1.18	0.35
3:00	0.81	0.85	−0.16	0.80	1.01	0.47
4:00	0.85	0.85	−0.19	0.85	0.81	0.33
5:00	0.86	0.79	−0.08	0.85	0.77	0.35
6:00	0.84	0.69	0.06	0.60	1.43	0.59
7:00	0.71	1.17	0.42	0.61	1.79	1.06
8:00	0.59	1.64	0.82	0.41	2.53	1.79
9:00	0.69	1.91	1.42	0.61	2.87	2.45
10:00	0.66	2.13	1.65	0.59	3.20	2.74
11:00	0.72	1.91	1.39	0.71	2.75	2.39
12:00	0.77	1.84	1.46	0.77	2.60	2.33
13:00	0.63	2.49	2.08	0.58	3.55	3.22
14:00	0.85	1.14	0.65	0.86	2.09	1.86
15:00	0.76	1.65	−0.65	0.68	1.75	0.36
16:00	0.78	1.97	−1.37	0.78	1.41	−0.11
17:00	0.67	2.53	−1.83	0.59	2.04	−0.73
18:00	0.57	2.67	−1.79	0.38	2.53	−0.76
19:00	0.63	2.50	−1.64	0.49	2.31	−0.70
20:00	0.67	1.78	−0.66	0.56	1.90	−0.02
21:00	0.66	1.61	−0.20	0.52	1.98	0.50
22:00	0.69	1.56	0.09	0.65	1.82	0.73
23:00	0.57	1.78	−0.15	0.57	1.85	0.47
24:00	0.77	1.30	0.05	0.66	1.70	0.73

4. Discussion

Water vapor density estimation from microwave links can be affected by environmental and technical interference factors. The efficient separation of gaseous attenuation from other signal losses will be challenging in practice. We have excluded rainy days to prevent the wet antenna effect, but the influences of fog and dew are difficult to eliminate without

the support of other observational data [16,17]. Recent work has suggested that, if multiple links at different frequencies are available, the need for side information can be relaxed [30]. Dew causing wetness on the antennas, and its contribution to the total attenuation for E-band microwave links can reach up to 4 dB [21]. The effect of absorption in oxygen significantly depends on temperature and pressure. There is an absorption in oxygen around the 60 GHz band, and the attenuation value of water vapor near this frequency is much less than that of dry air. Therefore, the retrieval of water vapor at approximately 60 GHz will be affected immensely by noise. Outside this frequency range, when the frequency is greater than 70 GHz and below 50 GHz, the attenuation of water vapor will significantly exceed that of dry air; this is a suitable frequency band for theoretical inversion of water vapor content [31]. Changes in atmospheric refractivity index may cause bending of the microwave ray and variations in received signal [32,33]. There are also uncertainties associated with the state of the underlying surface (temperature, roughness, land coverage, soil moisture, local water reservoirs, etc.) along the measuring route of the microwave links. For example, the E-band link in our study is located above the Gota River. While the microwave links measured the path-averaged water vapor density level, the humidity sensor of the weather station is a single point instrument, and it is not certain to represent the water vapor density along the entire link path. The measurement error of the humidity and temperature sensor of the weather station may also cause some deviation in the result. In addition, changes in temperature and humidity, as well as mechanical vibrations (strong winds), will affect the stability of the microwave link equipment and have an impact on the evaluation. Another important uncertainty factor is the attenuation quantization error, which has less impact on longer links. The retrieval model is also found to be sensitive on inaccurate temperature inputs, and errors in water vapor density estimation are proportional to the temperature bias [27].

5. Conclusions

The densely deployed millimeter-wave backhaul links in 5G cellular networks and smart cities have the great potential to provide high resolution water vapor density observations for improving weather monitoring and forecasts. It also can be used for investigation of the extreme events which are largely controlled by the humidity field, such as thunder storms and super cells, over continental regions. It is often the case when the humidity source is unclear; therefore, it is hard to predict where the storm is going to be and what its intensity will be.

We conducted water vapor density retrieval studies based on a month of data collected from commercial millimeter-wave links at 38 GHz and E-band located in the city center of Gothenburg, Sweden. The water vapor density derived from the millimeter-wave backhaul links is found to be accurate and, thus, provides a reliable observation. Especially, the WVD estimated from the 38 GHz link provides high correlation and in good agreement with that calculated from weather station measurements. Some sources of interference may affect the link-based water vapor density measurements. The weather station particularly installed for this study is located on the rooftop of a building, which is at one end of the link, and roof and ground humidity measurements may differ with altitude. There is no other weather station along the E-band link. The only weather station operated by the local weather agency in this area is far away from the E-band link, particularly. The measurements derived from the link represent the average water vapor density along the link, while the coverage of the weather station is rather limited. The E-band link is built above the city river, and one end of the link is on the bridge, so it is more prone to misalignment, wind, and a source of humidity below the link. Therefore, these factors need to be considered for water vapor density retrieval studies from millimeter-wave links, as well as can be useful for determining the most suitable links. It should be noted that land coverage, especially local water reservoirs, may have a dramatic effect on humidity, which could also lead to the differences between the two links. Rain can cause large attenuation over the signal link, and wetness on the antenna due to rain induces further attenuation. It is very challenging

to separate the signal attenuation due to change of rain intensity, water vapor level, and other factors during the rain or immediately after the rain. These uncertainty factors and limitations could be topics for future research.

Author Contributions: Conceptualization, C.H., L.B., G.S. and H.M.; methodology, C.H., L.B., H.M. and G.S.; software, C.H., L.B., G.S. and H.M.; validation, C.H., L.B., G.S. and H.M.; formal analysis, C.H., L.B. and G.S.; investigation, C.H., L.B., G.S. and H.M.; resources, L.B.; data curation, L.B.; writing—original draft preparation, C.H; writing—review and editing, C.H., L.B., G.S. and H.M.; visualization, C.H., L.B., G.S. and H.M.; supervision, L.B., C.H.; project administration, L.B., C.H.; funding acquisition, L.B., C.H. All authors have read and agreed to the published version of the manuscript.

Funding: This research was funded in part by National Natural Science Foundation of China (grant number 42027803, 41605122) and Suzhou Qiu Shi Technology Co., Ltd.

Institutional Review Board Statement: Not applicable.

Informed Consent Statement: Not applicable.

Data Availability Statement: The data presented in this study are available on request from the corresponding author. The data are not publicly available due to restrictions privacy.

Acknowledgments: The authors would like to specially thank Ericsson, Sweden for giving them access to data gratefully. The authors would also like to thank Pinhas Alpert and Yoav Rubin for helpful advice and discussions. The authors thanks anonymous reviewers for providing helpful advice.

Conflicts of Interest: The authors declare no conflict of interest.

References

1. Allan, R.P.; Shine, K.P.; Slingo, A.; Pamment, J.A. The dependence of clear-sky outgoing long-wave radiation on surface temperature and relative humidity. *Q. J. R. Meteorol. Soc.* **1999**, *125*, 2103–2126. [CrossRef]
2. Benton, G.S.; Blackburn, R.T.; Snead, V.O. The role of the atmosphere in the hydrologic Cycle. *Eos Trans. Am. Geophys. Union* **1950**, *31*, 61–93. [CrossRef]
3. Lennart, B. The global atmospheric water cycle. *Environ. Res. Lett.* **2010**, *5*, 1–8.
4. Emanuel, K.; Raymond, D.; Betts, A.; Bosart, L.; Thorpe, A. Report of the first prospectus development team of the U.S. Weather Research Program to NOAA and the NSF. *Bull. Am. Meteorol. Soc.* **1995**, *76*, 1194–1208.
5. Ducrocq, V.; Ricard, D.; Lafore, J.P.; Orain, F. Storm-scale numerical rainfall prediction for five precipitating events over France: On the importance of the initial humidity field. *Weather. Forecast.* **2002**, *17*, 1236–1256. [CrossRef]
6. Soden, B.J.; Turner, D.D.; Lesht, B.M.; Miloshevich, L.M. An analysis of satellite, radiosonde, and lidar observations of upper tropospheric water vapour from the atmospheric radiation measurement program. *J. Geophys. Res. Atmos.* **2004**, *109*, 1–19. [CrossRef]
7. Cady-Pereira, K.E.; Shephard, M.W.; Turner, D.D.; Mlawer, E.J.; Clough, S.A.; Wagner, T.J. Improved daytime column-integrated precipitable water vapor from Vaisala radiosonde humidity sensors. *J. Atmos. Ocean. Technol.* **2008**, *25*, 873–883. [CrossRef]
8. Jedlovec, G.J. Precipitable water estimation from high-resolution split window radiance measurements. *J. Appl. Meteorol.* **1990**, *29*, 863–877. [CrossRef]
9. Liljegren, J.C.; Clothiaux, E.E.; Mace, G.G.; Kato, S.; Dong, X. A new retrieval for cloud liquid water path using a ground-based microwave radiometer and measurements of cloud temperature. *J. Geophys. Res. Atmos.* **2001**, *106*, 14485–14500. [CrossRef]
10. Chen, B.; Liu, Z. Global water vapor variability and trend from the latest 36 year (1979 to 2014) data of ECMWF and NCEP reanalysis, radiosonde, GPS, and microwave satellite. *JGR Atmos.* **2015**, *121*, 11442–11462.
11. Messer, H.; Zinevich, A.; Alpert, P. Environmental monitoring by wireless communication networks. *Science* **2006**, *312*, 713. [CrossRef] [PubMed]
12. Alpert, P.; Messer, H.; David, N. Mobile networks aid weather monitoring. *Nature* **2016**, *537*, 617. [CrossRef] [PubMed]
13. Uijlenhoet, R.; Overeem, A.; Leijnse, H. Opportunistic remote sensing of rainfall using microwave links from cellular communication networks. *Wiley Interdiscip. Rev. Water* **2018**, *5*, e1289. [CrossRef]
14. Han, C.; Duan, S. Impact of atmospheric parameters on the propagated signal power of millimeter-wave bands based on real measurement data. *IEEE Access* **2019**, *7*, 113626–113641. [CrossRef]
15. David, N.; Alpert, P.; Messer, H. Novel method for water vapour monitoring using wireless communication networks measurements. *Atmos. Chem. Phys.* **2009**, *9*, 2413–2418. [CrossRef]
16. Alpert, P.; Rubin, P. First daily mapping of surface moisture from cellular network data and comparison with both observations/ECMWF product. *Geophys. Res. Lett.* **2018**, *45*, 8619–8628. [CrossRef]

17. Rubin, Y. A Novel Approach for High Resolution Humidity Mapping based on Cellular Network Data. Master's Thesis, Tel Aviv University, Tel Aviv, Israel, 2018.
18. Ericsson Mobility Report. 2018. Available online: https://www.ericsson.com/assets/local/microwave-outlook/documents/ericsson-microwave-outlook-report-2018.pdf (accessed on 4 August 2021).
19. Taori, R.; Sridharan, A. Point-to-multipoint in-band mmwave backhaul for 5G networks. *IEEE Commun. Mag.* **2015**, *53*, 195–201. [CrossRef]
20. Han, C.; Huo, J.; Gao, Q.; Su, G.; Wang, H. Rainfall monitoring based on next-generation millimeter-wave backhaul technologies in a dense urban environment. *Remote Sens.* **2020**, *12*, 1045. [CrossRef]
21. Fencl, M.; Dohnal, M.; Valtr, P.; Grabner, M.; Bareš, V. Atmospheric observations with E-band microwave links—Challenges and opportunities. *Atmos. Meas. Tech.* **2020**, *13*, 6559–6578. [CrossRef]
22. Rappaport, T.S.; Heath, R.W., Jr.; Daniels, R.C.; Murdock, J.N. *Millimeter Wave Wireless Communications*; Pearson/Prentice Hall: Hoboken, NJ, USA, 2015; pp. 99–110.
23. Rappaport, T.S.; MacCartney, G.R., Jr.; Samimi, M.K.; Sun, S. Wideband millimeter-wave propagation measurements and channel models for future wireless communication system design. *IEEE Trans. Commun.* **2015**, *63*, 3029–3056. [CrossRef]
24. International Telecommunication Union Radio Communication Bureau. *ITU-R P. 676–12 (International Telecommunication Union Radio Communication Bureau Propagation Recommendation). Attenuation by Atmospheric Gases and Related Effects*; International Telecommunication Union Radio Communication Bureau: Geneva, Switzerland, 14 August 2019.
25. Liebe, H.J.; Hufford, G.A.; Cotton, M.G. Propagation modeling of moist air and suspended water/ice particles at frequencies below 1000 GHz. In Proceedings of the AGARD Conference Proceedings of Electromagnetic Wave Propagation Panel Symposium, Boulder, CO, USA, 17–20 May 1993.
26. Liebe, H.J. An updated model for millimeter-wave propagation in moist air. *Radio Sci.* **1985**, *20*, 1069–1089. [CrossRef]
27. Fencl, M.; Dohnal, M.; Bares, V. Retrieval water vapor from E-band microwave link with an empirical model not requiring in situ calibration. *Earth Space Sci.* **2021**, *8*, e2021EA001911. [CrossRef]
28. Davis Wireless Vantage Pro2 Weather Station 6322. Available online: https://www.davisnet.com/weather-monitoring/ (accessed on 30 October 2021).
29. SMHI. Available online: http://www.smhi.se/en/weather/sweden-weather/observations#ws=wpt-a,proxy=wpt-a,tab=vader,param=t (accessed on 30 August 2021).
30. Tsidkiahu, D. Fog Classification based on Commercial Microwave Link Data. Master's Thesis, Tel Aviv University, Tel Aviv, Israel, 2019. Available online: https://web2.eng.tau.ac.il/wtest/rainlinklab/wp-content/uploads/2020/08/Thesis_Tsidkiahu_David_after_examRS.pdf (accessed on 15 January 2022).
31. Pu, K.; Liu, X.; Liu, L.; Gao, T. Water vapor retrieval using commercial microwave links based on the LSTM network. *IEEE J. Sel. Top. Appl. Earth Obs. Remote Sens.* **2021**, *14*, 4330–4338. [CrossRef]
32. David, N.; Sendik, O.; Rubin, Y.; Messer, H.; Gao, H.O.; Rostkier-Edelstein, D.; Alpert, P. Analyzing the ability to reconstruct the moisture field using commercial microwave network data. *Atmos. Res.* **2019**, *219*, 213–222. [CrossRef]
33. International Telecommunication Union Radio Communication Bureau. *ITU-R P. 453–11 (International Telecommunication Union Radio Communication Bureau Propagation Recommendation). The Radio Refractive Index: Its Formula and Refractivity Data*; International Telecommunication Union Radio Communication Bureau: Geneva, Switzerland, 29 July 2015.